ASTRONOMY & ASTROPHYSICS
SUPPLEMENT SERIES

DECEMBER II **1998**, PAGE 381

Astron. Astrophys. Suppl. Ser. **133**, 381–386 (1998)

The density and shock characteristics of NGC 2818⋆

J.P. Phillips[1] **and L. Cuesta**[2]

[1] Instituto de Astronomia y Meteorologia, Avenida Vallarta 2602, Col. Arcos Vallarta, C.P. 44130 Guadalajara, Jalisco, Mexico
e-mail: jpp@udgserv.cencar.udg.mx
[2] Instituto de Astrofisica de Canarias, La Laguna, Tenerife, Spain
e-mail: lcc@ll.iac.es

Received January 26; accepted June 26, 1998

Abstract. We report the results of narrow band imaging of the bipolar outflow source NGC 2818 in transitions of [NII], [OIII], [SII], and HI. As a consequence, we are able to assess the overall excitation properties of the shell, and determine that line ratios towards the nebular periphery are anomalous, and characteristic of planar shocks with velocity $V_{\rm s} \geq 110$ km s^{-1}. Pre-shock densities are likely to be modest, and of order $10^2 < n_{\rm p} < 10^3$ cm^{-3}.

The [SII] imaging is further used to derive a fully-sampled map of electron density, whence it is clear that the density structure is rather complex and related to various features within the excitation maps. Peak values $n_{\rm e} \sim 1.5\ 10^3$ cm^{-3} occur close to the nucleus, although densities subsequently decline for major axis displacements > 7 arcsec. The minor axis distribution, on the other hand, appears to be somewhat more extended and bilobal.

It is probable that complexities in the density mapping reflect the presence of condensations and filaments within the primary shell structure, and that these are also responsible for apparent variations in density as a function of forbidden and permitted line transition.

Key words: planetary nebula: NGC 2818 — ISM: jets and outflows

1. Introduction

The bipolar outflow NGC 2818 appears to possess many of the common characteristics of type I planetary nebulae, including anomalous abundances of He, C, and N, a high excitation spectrum (Dufour 1984), and a complex, filamentary sub-structure (e.g. Johnson 1969; Dufour 1984). It is however unusual among such nebulae in being located within a Population I galactic cluster of the same name; its position, extinction and radial velocity are all consistent with cluster membership (Tifft et al. 1972).

This should, in turn, permit a more precise analysis of the source physical characteristics, since cluster distances can be rather precisely determined (in principle) given a combination of stellar photometry and evolutionary theory. In reality, it appears that estimates for the distance of NGC 2818 have varied widely over the years, from 5 kpc (Shapley 1930), to 1.44 kpc (Barkhatova 1950), 3.2 and 3.5 kpc (respectively Tifft 1987 et al. 1972 and Dufour 1984), and more recently $D = 2.3$ kpc (Pedreros 1989).

Taking this latter (and more rigorous) value would imply a nebular mass $\approx 0.22 \Rightarrow 0.48\ M_\odot$ and unusually large dimensions $\Delta\alpha \times \Delta\delta = 1.44 \times 0.67$ pc^2, whilst the initial stellar mass was probably $2.2 \pm 0.3\ M_\odot$ (based on observed main-sequence turn-off: Dufour 1984). This mass is consistent with the range expected for type I progenitors (Peimbert & Torres-Peimbert 1983). Such stars are expected to possess electron-degenerate helium cores immediately following the main-sequence evolution (Iben & Renzini 1983).

Bannerjee et al. (1990) and Meatheringham et al. (1988) find expansion velocities $V_{\rm exp} \cong 20$ to 27 km s^{-1} (although the estimates of Dufour (1984) appear to be $\sim$ twice as large). Bannerjee et al. also note a considerable complexity in the low-excitation line structure. Whilst Boffi & Stanghellini (1994) determine a filling factor $\varepsilon = 0.22$, both Kohoutek et al. (1986) and Dufour (1984) assign lower values $\varepsilon = 0.03$ to 0.055 on the basis of forbidden line/Hα ratios, and inspection of direct nebular imaging. Pedreros (1989) apparently prefers an intermediate value $\varepsilon = 0.121$. Such results are consistent with imaging in suggesting a highly filamentary and/or fragmented shell; a characteristic which may also help to explain variations in the electron densities determined from forbidden lines, which appear to range between $n_{\rm e}({\rm S}^+) \cong 430$ cm^{-3} and $n_{\rm e}({\rm Cl}^{++}) \cong 1300$ cm^{-3} (Dufour 1984; see also Torres-

Send offprint requests to: J.P. Phillips

⋆ Figure 5 in colour is only available at the http://edpsciences.com

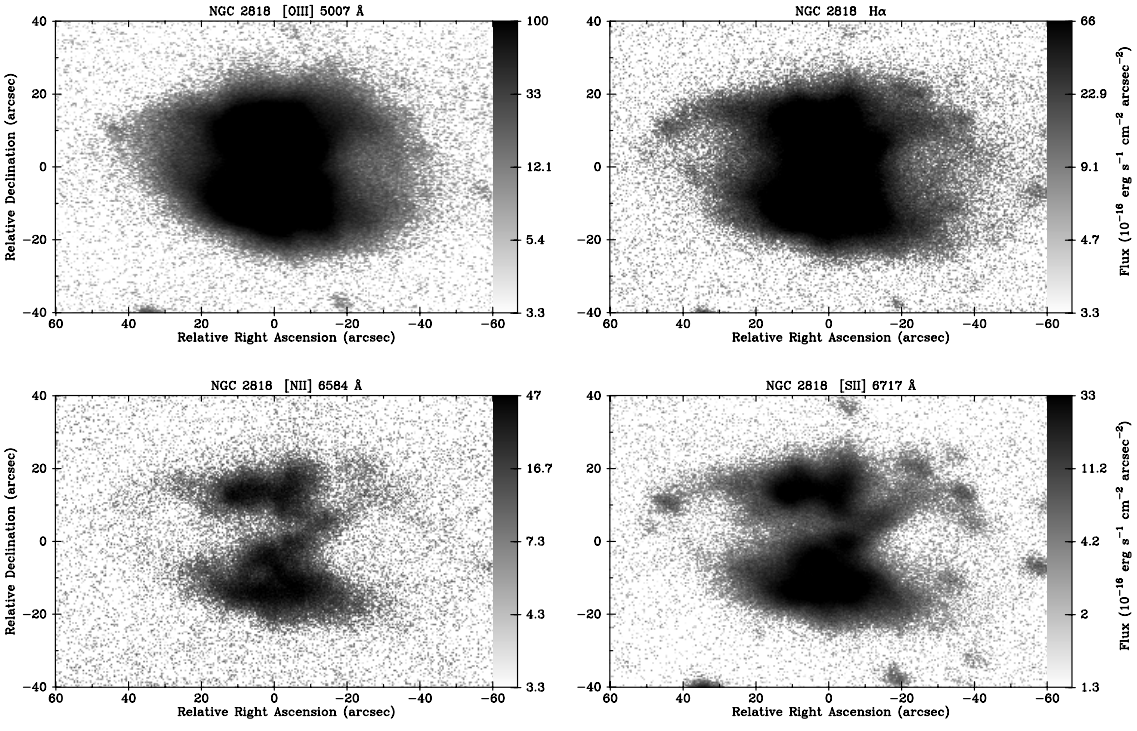

Fig. 1. Direct imaging of NGC 2818 in the transitions [NII] λ6584 Å, [OIII] λ5007 Å, HI λ6563 Å, and [SII] $\lambda\lambda$6717 Å+ 6731 Å. Note the presence of E−W arm-like features extending on either side of the core, and the apparent increased levels of complexity in the lower excitation images

Peimbert & Peimbert 1977). The mean density deduced from the Hβ intensities is of order $117-140\,\mathrm{cm}^{-3}$ (Dufour 1984; Torres-Peimbert & Peimbert 1977).

Finally, the shell appears also to be associated with strong H_2 $S(1)$ $\lambda = 2.1$ μm quadrupole emission, suggesting the presence of (possibly UV excited) neutral gas within the principal ionised shell, and shock-excited material immediately adjacent (but external to) the southerly ionised limits to the source (Schild 1995).

It is apparent, therefore, that NGC 2818 is an unusually interesting example of the bipolar outflow phenomenon. We provide, below, the first detailed investigation of the excitation structure of this outflow, together with a fully-sampled map of electron density extending over most of the primary shell.

2. Observations

The present observations were acquired using the 1.5 m f/13.5 Johnson telescope at the Observatorio Astronomico Nacional at San Pedro Martir, Baja California, Mexico. A Thomson 2048 × 2048 CCD was used to obtain images of the source in [NII] λ6584 Å, [OIII] λ5007 Å, HI λ6563 Å, and [SII] $\lambda\lambda$6717 Å and 6731 Å at a plate scale of 0.4 arcsec pixel^{-1}.

Seeing was poor (of order 2 arcsec) but consistent, whilst flux calibration was performed using BD+8°2015 and Kopff 27, whose continuum fluxes are quoted by Stone (1977). An alternative calibration was available in the case of the [SII] filters (used to derive the density map in Fig. 5), since the field stars have closely comparable fluxes at the wavelengths $\lambda\lambda$6731 Å and 6717 Å of the [SII] doublet.

The images were subsequently processed using the Figaro package, and are presented in Fig. 1. In addition, the individual [SII] λ6717 and λ6731 images were ratiod with each other, and the resulting matrix converted into a map of projected densities illustrated in Fig. 5.

3. Excitation structure

Emission maps of NGC 2818 are shown in Fig. 1 for a variety of ionic transitions. It is clear that the source possesses a bipolar structure reminiscent of certain other type I outflows, including Mz 1, IC 4406, and M 1−8 (e.g. Corradi & Schwartz 1995). Similarly, although the resolution of the images is only moderate, it is apparent that the lower-excitation [NII] and [SII] structures appear significantly more complex than for HI and [OIII].

Such variations are also evident in Fig. 2, where we display spatial profiles along the minor axes (PA = 85°). The minor axis emission has a double-peaked structure. The southern low excitation peaks (i.e. those in [NII] and [SII]) appear broader than their higher excitation counterparts. This disparity, as we shall note later, may

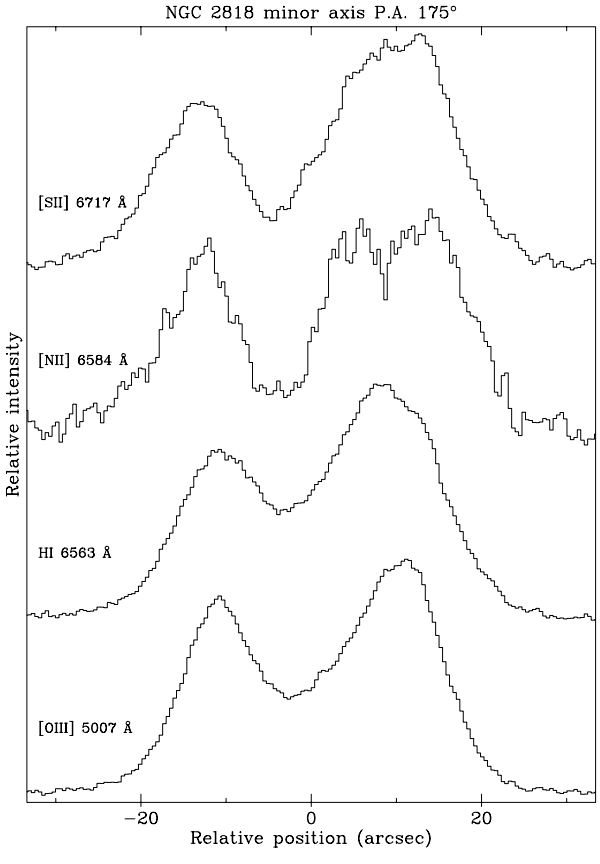

Fig. 2. Minor axis profiles in line intensity for various ionic transitions, whence it may be noted that the low and higher excitation transitions are characterised by markedly differing structures. Note the greater extension of the lower excitation transitions towards the south (positive axial displacements), close to a region where H_2 $S(1)$ emission appears also to be enhanced (Schild 1995)

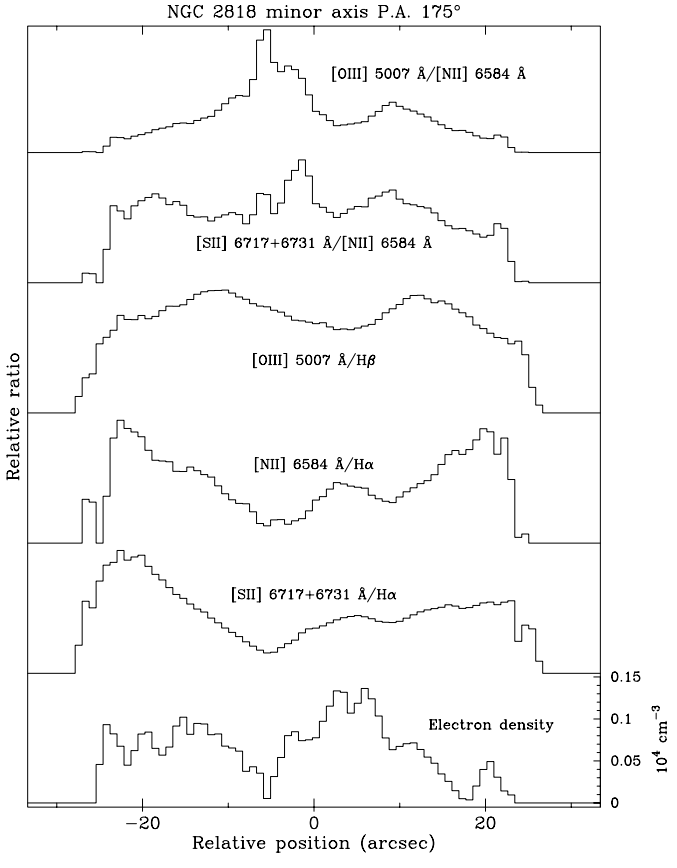

Fig. 3. Spatial variations in line ratio along the nebular minor axis, together (bottom) with the corresponding trend in electron density n_e

reflect local shock-enhancement of the lower excitation transitions.

Line ratio variations along the minor axis are illustrated in Fig. 3, whilst line-ratio maps are presented in Figs. 4 and 5. The [OIII]/Hα emission peaks in an annulus, whilst lower excitation conditions prevail towards the nucleus and in the outer shell.

The ratios to Hα of the low-excitation lines ([NII] and [SII]: Fig. 4) show the same complexity as in direct imaging (Fig. 1), with barely resolved line-ratio enhancements occurring at various locations within the projected shell structure. Note, particularly, the high [SII]/Hα ratios near the northern limits of the source.

4. Shell density mapping

The complexity displayed in Figs. 1 and 4 is also visible in the density map illustrated in Fig. 5, where we have employed images in [SII] λ6717 and λ6731 to determine n_e, and used a mean temperature T_e = 14500 K (relevant for [OIII], Dufour 1984). While this value may not be appropriate, the derived densities are relatively insensitive to T_e. The profile for the minor axis is illustrated in Fig. 3. Several features are noteworthy:

1) It is apparent that the variation in density is both marked and irregular, with regions of enhanced density correlating closely with increases in [SII] intensity and/or line ratio [SII]/Hα. The structure of the higher density regimes, in brief, is similar to the filamentary source structure evident from direct imaging.
2) The density contrast ratio for the filaments (that is, the ratio between densities in the filaments and those of the broader envelope) is at least ~ 2. Given that most of the filaments are only barely if at all resolved, the actual contrast ratios are probably much higher.
3) The density peaks at $\sim 1.2\ 10^3$ cm^{-3} close to the nucleus. This region may be an unresolved mix of filaments, however, and the value of n_e is probably a lower limit.
4) There appears to be a weak but suggestive connection in the northern part between minor axis [OIII]/Hα filaments, and some of the higher density ridges and condensations. It is conceivable that we are witnessing the effects of shock interaction between the primary shell and a collimated outflow. Such mechanisms may also explain

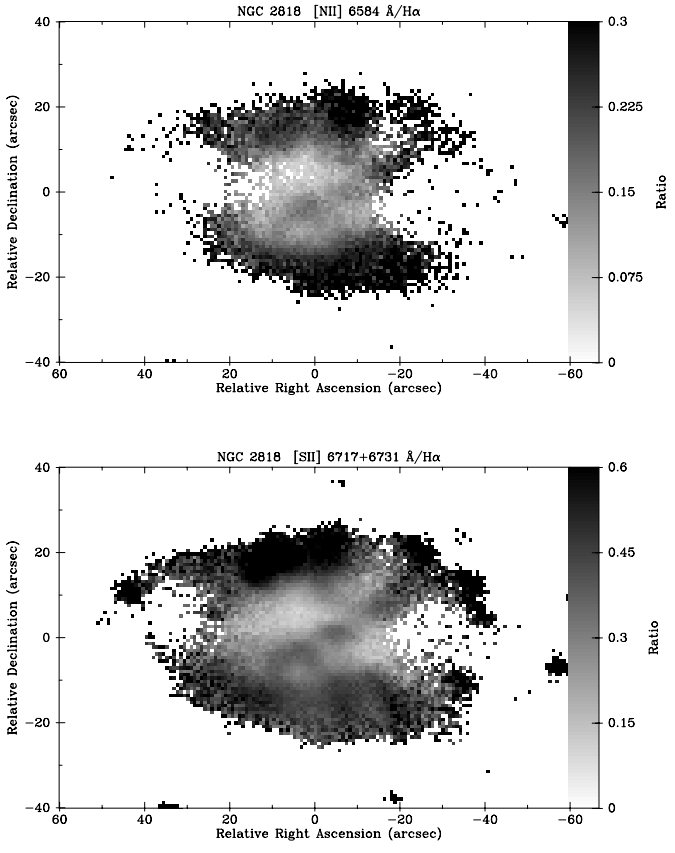

Fig. 4. Image of [SII]/Hα and [NII]/Hα ratios

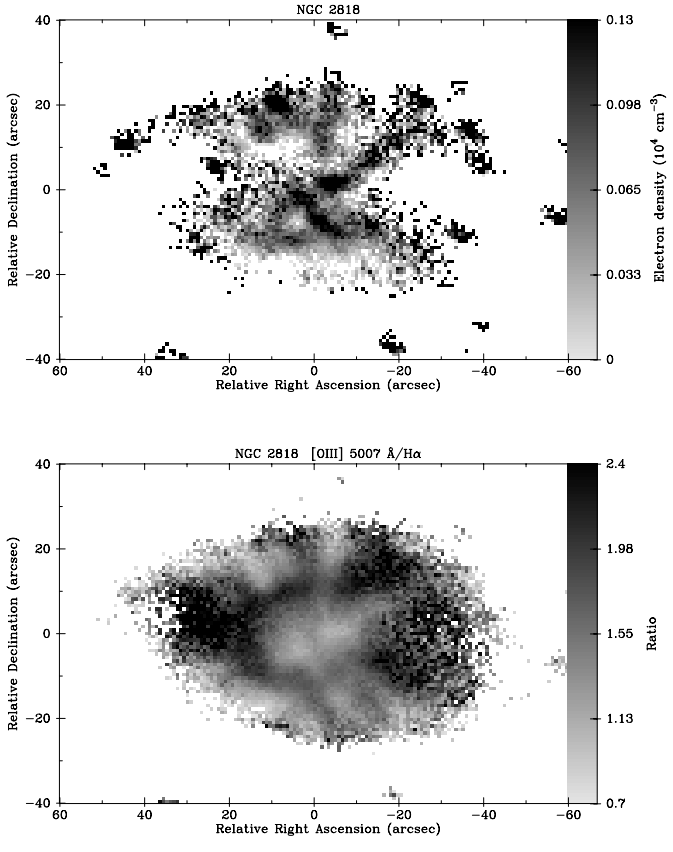

Fig. 5. Map of electron density (above) derived from the [SII] $\lambda\lambda$6717, 6731 Å images, whence it is clear that the shell density structure is rather irregular and complex. The map of [OIII]/Hα (below) implies that excitation trends are also complex, with higher excitation in an annular regime having $\Delta\alpha \times \Delta\delta$ 36 × 16 arcsec^2

point-reflection symmetries in other nebulae, and radially extended low excitation features in NGC 6210 and K 1−2 (Phillips & Cuesta 1996; Bond & Livio 1990).

5) There is no clear evidence for density enhancement close to the southerly limit of the ionised shell, as might be expected were appreciable shock compression to occur (see discussion in Sect. 5). This may, however, be a consequence of lower [SII] intensities in this regime, and of the corresponding difficulty in evaluating reliable [SII] line ratios.

5. Shock excitation in NGC 2818

As noted previously in Sect. 3, the [SII] and [OIII] profiles along the southern part of NGC 2818 appear to be significantly more extended than their higher excitation counterparts, a characteristic which results in enhanced [SII]/Hα and NII/Hα line ratios towards the nebular outer edge (Fig. 3). This region is also that of strongest (and probable shock excited) H_2 $S(1)$ emission observed by Schild (1995).

By contrast, the more northerly emission counterparts (where H_2 $S(1)$ emission is weaker) possess similar distributions in all transitions, although the ratios [NII]/Hα and [SII]/Hα again peak at large radial distances.

The correlation between the locations of shocked H_2 $S(1)$ and enhanced low excitation line ratios is at the very least suggestive, and may imply a similar shock origin for both optical and IR transitions. To evaluate this possibility, we have therefore indicated the location of the minor axis ratios [NII]/Hα and [SII]/Hα in a diagnostic diagram due to Sabbadin et al. (1977; Fig. 6). Although the data base employed by Sabbadin et al. appears not to have been corrected for extinction, the influence of reddening is probably very small.

Inspection of Fig. 6 suggests that the dereddened line ratios for NGC 2818 parallel the trend observed for normal PN, although they are in fact outside of the ranges expected for most emission line nebulae. There is no evidence here to support shock excitation, which might be expected to give ratios similar to those of supernova remnants (SNR).

By contrast, a rather different result is obtained where we compare the [SII]/Hα and [OIII]/Hα ratios with dereddened line ratios for "normal" planetary nebulae, and the values predicted for planar and bow-shocks (see Fig. 7, and the models of Hartigan et al. 1987, and Shull & McKee 1979). In constructing this diagram, we have employed a heterogeneous sample of 492 spectra derived from the

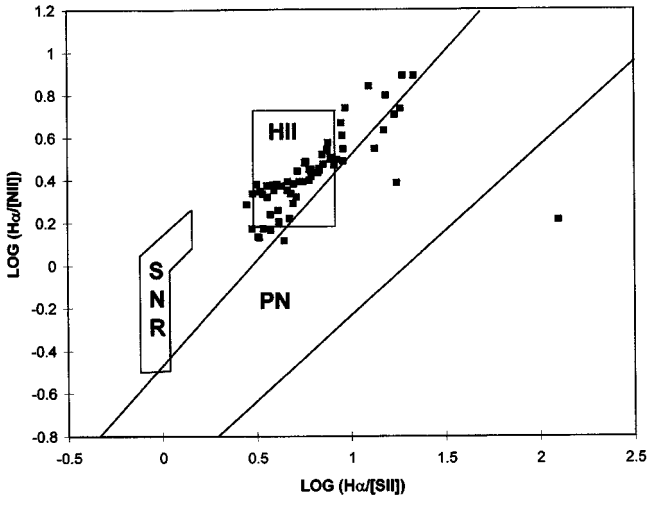

Fig. 6. Location of de-reddened minor axis ratios for NGC 2818 in an Hα/[NII] – Hα/[SII] diagram due to Sabbadin et al. (1977). Although the observed ratios parallel the regime for normal PN, they are outside of the ranges expected for most emission line nebulae

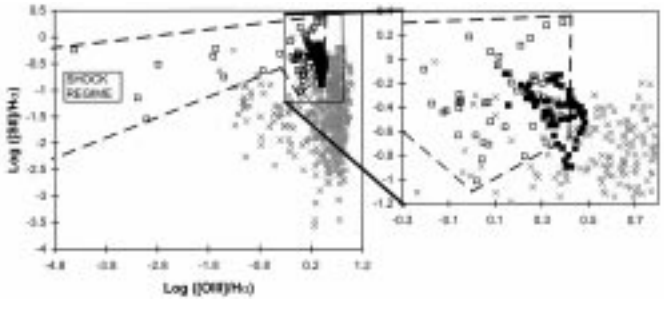

Fig. 7. Location of de-reddened minor axis ratios within the [SII]/Hα – [OIII]/Hα plane (■). It may be noted that core values for NGC 2818 (i.e. those at low radial offsets) occur at low values of [SII]/Hα ($\log([\mathrm{SII}]/\mathrm{H}\alpha) < -0.5$); those towards the south periphery of the source are located to the upper left; and those corresponding to northerly axial displacements are positioned to the upper right (i.e. typically $\log([\mathrm{SII}]/\mathrm{H}\alpha) > -0.5$, $\log([\mathrm{OIII}]/\mathrm{H}\alpha) > 0.35$). We also show, for comparison, de-reddened line ratios for a heterogeneous sample of "normal" PN (×), and results for planar- and bow-shock modelling due to Hartigan et al. (1987) and Shull & McKee (1979) (□). Note that line ratios towards the periphery of NGC 2818 appear to lie increasingly within the shock modelling regime

catalogue of Kaler et al. (1997), together extinctions compiled by Tylenda et al. (1992), and the extinction curve of Savage & Mathis (1979).

It is apparent, from Fig. 7, that whilst the line ratios with $\log([\mathrm{SII}]/\mathrm{H}\alpha) < -0.5$ (observed at the centre of NGC 2818) are similar to those for "normal" PN, the ratios in the outer parts are significantly greater, and extend into the regime defined by the shock modelling solutions. It seems likely, therefore, that these ratios are explicable by shock excitation.

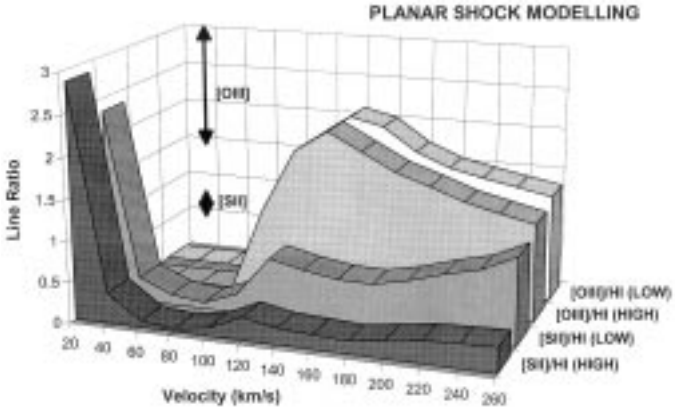

Fig. 8. Predicted variation in [OIII]/Hα and [SII]/Hα line ratios as a function of shock velocity, together (arrows) with the observed de-reddened ranges in these parameters towards the periphery of NGC 2818. We have indicated, separately, the trends anticipated for low (10^2 cm^{-3}) and high (10^3 cm^{-3}) pre-shock densities

The characteristics of the shocks responsible for this emission are difficult to identify with precision. Where shock excitation dominates, however, then one would expect to observe the trends in [SII]/Hα and [OIII]/Hα noted in Fig. 8; where the individual curves correspond to differing line ratios, and planar modelling solutions having high (10^3 cm^{-3}) and low (10^2 cm^{-2}) pre-shock densities (Hartigan et al. 1987; see labelling to the right). The observed ranges in the line ratios are indicated by vertical arrows in this figure.

Taken together, both sets of line ratio would imply values $V_\mathrm{s} \geq 110$ km s^{-1} or larger, associated (presumably) with some as yet unobserved high velocity wind. Similar high-velocity outflows have previously been noted in NGC 6537 (Cuesta et al. 1995), M 2 – 9, Hb5 (Phillips & Mampaso 1988), NGC 6302 (Meaburn & Walsh 1980) and several other bipolar sources (cf. Grewing 1988), and appear to constitute a primary mechanism for shaping nebular shells at relatively late stages of PN evolution. In particular, the interaction of such winds with superwind envelopes has been invoked to explain precisely those structures which appear to characterise the NGC 2818 morphology (e.g. Cuesta et al. 1993, 1995; Balick et al. 1987; Icke & Preston 1989; Icke et al. 1992), including the dual arm-like extensions on either side of the major axis (Fig. 1).

6. Conclusions

We have obtained narrow band imaging of the bipolar outflow source NGC 2818 in the transitions [NII] λ6584 Å, [OIII] λ5007 Å, HI λ6563 Å, and [SII] $\lambda\lambda$6717 Å and 6731 Å. As a result, it has proved possible to confirm the overall complexity in outflow structure noted by previous

authors, with filaments and condensations in the direct imaging having their counterparts in line-ratio mapping.

The map of projected electron density appears to be rather complex, and suggests the presence of higher density condensations and filaments within a lower density structure. Several of the density enhancements appear to be related to corresponding features in the excitation maps, and might constitute evidence for jet activity.

Of particular interest is an apparent extension in the [SII], [NII] minor axis structure towards the south, in a region where shocked H_2 $S(1)$ emission has previously been observed by Schild (1995). This (together with correspondingly enhanced [SII]/Hα, [NII]/Hα line ratios) may constitute evidence for shock excitation of optical transitions towards the nebular periphery. Comparison between the ratios [OIII]/Hβ, [SII]/Hβ and planar shock modelling implies that shock velocities are likely to be of order $V_{\rm s} \geq 110$ km s^{-1}, whilst pre-shock densities (neutrals + ions) are in the range 10^2 cm$^{-3} < n_{\rm p} < 10^3$ cm^{-3}, consistent with our density mapping.

Although an outflow with such velocities has not yet been observed in this source, it is conceivable that some such component explains the overall nebular morphology.

References

Balick B., Preston H.L., Icke V., 1987, AJ 94, 1641
Bannerjee D.P.K., Anandarao B.G., Jain S.K., Malli D.C.V., 1990, A&A 240, 137
Barhatova K.A., 1950, Astr. Zh. 27, 180
Boffi F.R., Stanghellini L., 1994, A&A 284, 248
Bond H.E., Livio M., 1990, ApJ 355, 568
Corradi R.L.M., Schwartz H.E., 1995, A&A 293, 871
Cuesta L., Phillips J.P., Mampaso A., 1993, A&A 267, 199
Cuesta L., Phillips J.P., Mampaso A., 1995, A&A 304, 475
Dufour R.J., 1984, ApJ 287, 341
Grewing M., 1988, in: IAU Symposium 131, S. Torres-Peimbert (ed.). Reidel, Dordrecht, Holland, p. 241
Hartigan P., Raymond J., Hartmann L., 1987, ApJ 316, 323
Iben I., Renzini A., 1983, ARA&A 21, 271
Icke V., Balick B., Frank A., 1992, A&A 253, 224
Icke V., Preston H.L., 1989, A&A 211, 409
Johnson H.M., 1969, PASP 72, 418
Kaler J.B., Shaw R.S., Browning L.B., 1997, PASP 109, 289
Kohoutek L., Roth-Höner M.L., Laustsen S., 1986, A&A 162, 232
Meaburn J., Walsh J.R., 1980, MNRAS 191, 5
Meatheringham S.J., Wood P.R., Faulkner D.J., 1988, ApJ 334, 862
Pedreros M., 1989, AJ 98, 2146
Phillips J.P., Cuesta L., 1996, AJ 111, 1227
Peimbert M., Torres-Peimbert S., 1971, ApJ 168, 413
Peimbert M., Torres-Peimbert S., 1983, in IAU Symposium 103, Planetary Nebulae, Flower D.R. (ed.). Dordrecht: Reidel, p. 391
Phillips J.P., Mampaso A., 1988, in: IAU Symposium 131, Torres-Peimbert S. (ed.). Reidel, Dordrecht, Holland, p. 194
Sabbadin F., Minello S., Bianchini A., 1977, A&A 60, 147
Savage B.D., Mathis J.S., 1979, ARA&A 17, 73
Schild H., 1995, A&A 297, 246
Shapley H., 1930, Star Clusters. McGraw-Hill, New York, p. 230
Shull J.M., McKee C.F., 1979, ApJ 227, 131
Stone R.P.S., 1977, ApJ 218, 767
Tifft W.G., Connolly L.P., Webb D.F., 1972, MNRAS 158, 47
Torres-Peimbert S., Peimbert M., 1977, Rev. Mex. Astron. Astrofis. 2, 181
Tylenda R., Acker A., Stenholm B., Koppen J., 1992, A&AS 95, 337